Modeling and Simulation of a PMSM Drive System for Electric Vehicles Using Finite Control Set Model Predictive Controller

Rafael dos Santos
Fabrício Leonardo Silva
Institute of Science and Technology of Sorocaba - São Paulo State University - UNESP, Sorocaba, Brazil

ABSTRACT

The electrification of vehicles has emerged as a promising solution to reduce pollutant emissions and dependence on fossil fuels, aligning with global demands for sustainable mobility. In this context, the development of innovative technologies for electric vehicles (EVs) is essential to enhance efficiency, performance, and economic viability. One of the critical aspects for the success of these vehicles is the control of the electric motor drive system, which is an essential part of the EV electrical propulsion structure. Therefore, this work aims to model and simulate a Permanent Magnet Synchronous Motor (PMSM) drive system considering the vehicle dynamics. Additionally, the PMSM current control is performed using a Finite Control Set Model Predictive Control (FCS-MPC) which allows a faster and more robust motor dynamic response. The validation of the motor drive system with the FCS-MPC controller will be conducted through a driving cycle, which will assess the ability of the proposed electric propulsion system to reproduce the desired behavior throughout the cycle accurately.

INTRODUCTION

The increasing concerns about pollution and climate change have driven significant transformations in various sectors of society. In the automotive industry, these changes are aimed at revolutionizing both urban mobility and freight transport, with a focus on reducing dependence on fossil fuels [1], [2]. The increase in the concentration of greenhouse gases in the atmosphere, resulting mainly from the burning of these fuels, has led governments and international organizations to set increasingly stringent decarbonization targets [3], [4].

In Brazil, the National Program for Green Mobility and Innovation (Mover) aims to accelerate the transition to more efficient and sustainable vehicles, fostering technological advancement in the automotive industry [5]. The initiative offers tax incentives and supports research, development, and innovation projects. Additionally, it promotes the strengthening of the national production chain, the use of biofuels, and low-emission technologies, directly contributing to the decarbonization of the sector [5].

In this context, electric vehicles (EVs) have emerged as one of the leading alternatives for the future of sustainable mobility, as they enable the reduction of atmospheric pollutant emissions and contribute to improved air quality in urban centers [6]. These vehicles rely on a propulsion system composed of electric motors and rechargeable batteries. When properly designed and controlled, EVs can achieve high energy efficiency, offer lower operational costs, and operate with zero direct pollutant emissions [7].

Among the various types of electric motors used in electromobility, including Brushless DC Motors, Induction Motors and Synchronous Reluctance Motors [8]; Permanent Magnet Synchronous Motors (PMSMs) stand out for their high efficiency, high power density, and superior dynamic response [9]. These characteristics make PMSMs particularly attractive for automotive applications, where requirements such as high torque, precise control, and energy efficiency are essential.

Various control strategies can be employed in the management of electric propulsion systems, with the decision of approach depending on the system's complexity as well as performance and robustness requirements. In the context of EVs, several techniques have been extensively explored in the literature, such as proportional-integral-derivative (PID) controllers [10] [11], fuzzy logic control (FLC) [12] [13] , artificial neural networks (ANN) [14], and model predictive control (MPC) [15], as shown in Tab. 1. Although PID controllers are simple and widely used, they exhibit limitations when applied to nonlinear dynamic systems. On the other hand, the FLC and the ANN offer better performance in nonlinear systems and greater adaptability to varying operating conditions, although they require more effort for implementation and training [16] [14]. MPC stands out due to its ability to handle system constraints and predict the future behavior of the plant, making it particularly attractive for applications demanding high efficiency, dynamic response, and operational safety [15]. Therefore, selecting an appropriate control technique is essential for the development of more efficient, safe, and reliable electrified propulsion systems.

Considering the demand for technologies that promote vehicle electrification and the need for more efficient and robust control strategies for electric propulsion systems, this

Table 1. Literature review applied to EVs control strategies

Control	Reference	Application
PID	Dantas et al. [10]	PID control for DC motors in electric vehicles with independent excitation and constant field current. The controller tuning was performed using controlled invariant set and multiparametric programming techniques, ensuring compliance with the motor's physical constraints, such as angular velocity limits and armature voltage
	Shamseldin [11]	Speed control for electric motors in EVs using a nonlinear PID controller. The system employs optimization techniques to automatically tune the controller, enhancing the vehicle's dynamic performance and reducing energy consumption.
FLC	Miranda et al. [12]	FLC strategy for power distribution management in four-wheel independent drive electric vehicles. The FLC parameter tuning is performed using multi-objective optimization techniques based on a particle swarm optimization algorithm.
	Eckert et al. [13]	Power distribution control system for a hybrid energy storage system composed of batteries and ultracapacitors. The control strategy implements fuzzy logic, with parameters optimized through multi-objective genetic algorithm optimization techniques
ANN	Silva [14]	An ANN-based energy management control strategy is developed for electric vehicle propulsion systems. The ANN training is performed using genetic algorithm optimization techniques
MPC	He et al. [15]	Energy management strategy based on MPC for electrified bus propulsion systems. The controller determines optimal power distribution with enhanced predictive accuracy and optimized speed sequences by integrating vehicle-to-vehicle and vehicle-to-infrastructure communication data.

work aims to develop, model, and simulate a drive system based on a PMSM, taking into account vehicle dynamics. The proposed approach includes the implementation of a Finite Control Set Model Predictive Control (FCS-MPC) strategy for motor current control, aiming to enhance the dynamic response and overall performance of the traction system. Validation is carried out through the application of a driving cycle, allowing the assessment of the proposed system's ability to accurately reproduce the desired behavior during operation.

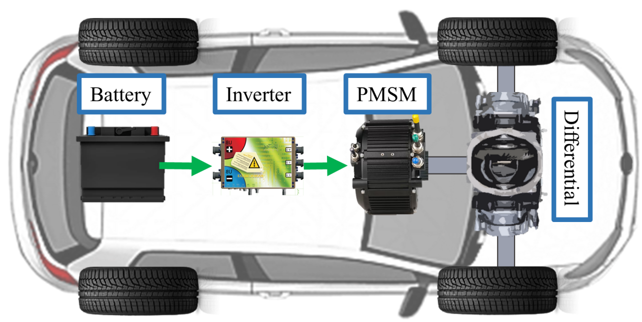

Figura 1. The electric vehicle configuration

ELECTRIC VEHICLE MODEL

The electric vehicle configuration considered in this study is illustrated in Figure 1. The vehicle is powered by a PMSM, which is coupled to a differential that transmits torque to the drive wheels.

In order to understand the longitudinal behavior of a vehicle in motion, it is essential to identify and quantify the forces acting along the direction of travel, as presented in Fig. 2. In general, two main groups of forces influence the vehicle's movement: the traction force F_{tr} [N], generated by the powertrain to propel the vehicle, and the resistive forces R_{res} [N], which oppose its motion [17]. By applying Newton's Second Law to the longitudinal dynamics of the vehicle, the net force is equal to the product of the vehicle's mass m [kg] and its longitudinal acceleration a_x [m/s²], as expressed in Eq. 1.

$$F_{\text{tr}} - R_{\text{res}} = m a_x \tag{1}$$

The total resistance to vehicle motion consists mainly of three components: aerodynamic drag R_{aero} [N], rolling resistance R_{rr} [N], and the resistance due to road gradient R_{ri} [N] (Fig. 2). Therefore, the overall resistive force acting on the vehicle can be described by Eq. 2 [18].

$$R_{\text{res}} = R_{\text{aero}} + R_{\text{rr}} + R_{\text{ri}} \tag{2}$$

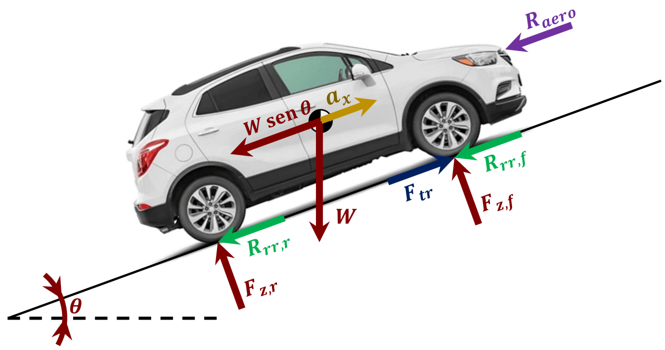

Figura 2. Forces acting on the vehicle

The resistance associated with the road gradient corresponds to the component of the vehicle's weight projected along the direction of movement. This force is proportional to the sine of the road slope angle θ [°], as shown in Eq. 3. In situations where the road descends ($\theta < 0$), this component acts in favor of the motion, thereby enhancing the vehicle's acceleration [17].

$$R_{\text{ri}} = mg\sin(\theta) \tag{3}$$

Aerodynamic resistance is associated with the drag generated by air flowing around the vehicle's body. Its magnitude depends on the air density ρ [kg/m³], the vehicle's drag coefficient C_d, its frontal area A_f [m²], and the longitudinal velocity V_x [m/s], as indicated in Eq. 4 [19].

$$R_{\text{aero}} = \frac{1}{2}\rho A_f C_d V_x^2 \tag{4}$$

Rolling resistance results from the deformation of the tires over the road surface during movement. This force is proportional to the vehicle's weight and is influenced by the inclination of the road, as defined in Eq. 5 [18].

$$R_{\text{rr}} = f_{\text{r}} mg\cos(\theta) \tag{5}$$

The rolling resistance coefficient f_{r} depends on several factors, including tire construction and condition, inflation pressure, pavement type, and surface characteristics. Among these, vehicle speed is the parameter with the greatest influence on rolling resistance. Hence, the rolling resistance coefficient can be expressed as a linear function of velocity, consisting of a constant term f_0 and a velocity-dependent term f_1, as represented in Eq. 6 [18].

$$f_{\text{r}} = f_0 + f_1 V_x \tag{6}$$

From the vehicle's current speed V_x [m/s], the target speed V_d [m/s], and a predefined time interval dt [s] to reach that speed, it is possible to estimate the required acceleration a_{req} [m/s²], as shown in Eq. 7.

$$a_{\text{req}} = \frac{V_d - V_x}{dt} \tag{7}$$

The required wheel torque $T_{w,\text{req}}$ [Nm] to achieve this acceleration can be obtained from Eq. 1, and is expressed in Eq. 8.

$$T_{w,\text{req}} = r_p\left(ma_{\text{req}} + R_{\text{aero}} + R_{\text{rr}} + R_{\text{ri}}\right) \tag{8}$$

On the other hand, the torque at the wheel T_w [Nm] can also be expressed as a function of the electric motor torque T_{ME} [Nm], taking into account the motor inertia I_{ME} [kg·m²], the differential gear ratio N_d, the differential inertia I_d [kg·m²], and the equivalent inertia of the wheel-tire assembly I_w [kg·m²], as shown in Eq. 9 [19].

$$T_w = T_{\text{ME}}N_d - \left((I_{\text{ME}} + I_d)N_d^2 + I_w\right)\frac{a_x}{r_p} \tag{9}$$

The transmitted wheel torque must not exceed the maximum transmissible torque $T_{\max}$ [Nm], which represents the adhesion limit between the tire contact patch and the road surface. This maximum torque can be estimated by Eq. 10, as a function of the tire's dynamic radius r_p [m], the vertical load F_z [N] on the tire, and the friction coefficient μ [17].

$$T_{\max} = \mu F_z r_p \tag{10}$$

During acceleration and braking moments, there is a longitudinal load transfer between the vehicle's axles. According to Genta [17], this load transfer ΔF_z can be estimated based on the longitudinal acceleration a_x [m/s²], the vehicle mass m [kg], the wheelbase l [m], the road inclination angle θ [°], and the height of the center of gravity h_{cg} [m], as shown in Eq. 11.

$$\Delta F_z = \frac{mh_{\text{cg}}}{2l}\left(a_x + g\sin(\theta)\right) \tag{11}$$

Consequently, the normal loads on the front axle $F_{z,d}$ [N] and the rear axle $F_{z,t}$ [N] can be calculated by considering the longitudinal position of the center of gravity x_{cg} [m] and the load transfer. The normal forces on each axle are given by Eqs. 12 and 13.

$$F_{z,f} = mg\cos(\theta)\frac{(l - x_{\text{cg}})}{l} - \Delta F_z \tag{12}$$

$$F_{z,r} = mg\cos(\theta)\frac{x_{\text{cg}}}{l} + \Delta F_z \tag{13}$$

Finally, all relevant vehicle parameters are summarized in Tab. 2 [17].

Table 2. Simulated vehicle parameters [17].

Parameter		Value
Total vehicle mass	(m)	980 kg
Wheelbase	(l)	2.6 m
Gravity center height	(h_{cg})	0.545 m
The longitudinal position of the CG	(x_{cg})	1.400 m
Vehicle frontal area	(A_f)	2.18 m^2
Drag coefficient	(C_d)	0.32
Linear coefficient of rolling resistance	(f_0)	0.0100
Angular coefficient of rolling resistance	(f_1)	0.0002
Tire peak friction coefficient	(μ)	0.9
Dynamic tire radius	(r_p)	0.307 m
Wheel inertia	(I_ω)	0.860 kgm^2
Diferential inertia	(I_ω)	0.135 kgm^2
Differential gear ratio	(I_ω)	5

DRIVING CYCLE

To develop and evaluate the performance of the control strategy applied to the vehicle's electrified drivetrain, standardized driving cycles were employed. These driving cycles are essential as they allow for the consistent execution of tests and experiments across different vehicles, enabling a more reliable comparison of results.

The standard driving cycles selected to support the development of the FCS-MPC control approach are the FTP-75 and HWFET cycles. The FTP-75 cycle, shown in Figure 3, is designed to represent urban driving conditions. In Brazil, it is the primary cycle used for vehicle emissions testing and is described in the NBR 6601 standard.

The HWFET cycle, presented in Figure 4, on the other hand, was developed to characterize highway driving conditions and is defined in the NBR 7024 standard. Therefore, the test cycle used in this study is a combination of both FTP-75 and HWFET, ensuring that the control strategy addresses both urban and highway driving scenarios.

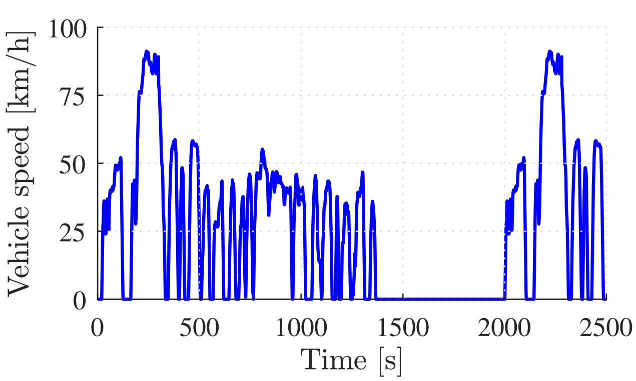

Figura 3. FTP-75 driving cycles

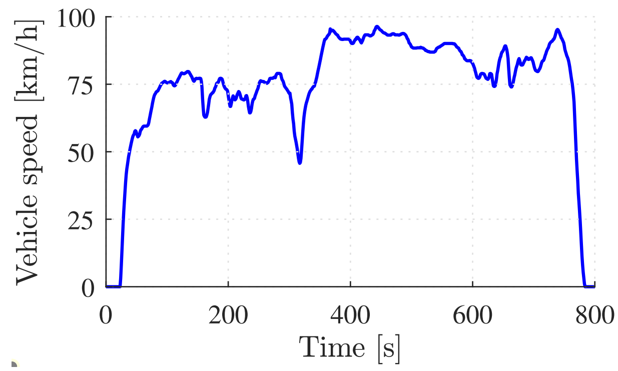

Figura 4. HWFET driving cycles

ELECTRIC MOTOR MODEL

The electric machine selected to generate mechanical power and drive the vehicle is a Permanent Magnet Synchronous Motor (PMSM), model EMRAX 208 [20]. In the rotor reference frame (qd frame), the differential equations that describe the dynamics of PMSM are described by (15)-(16), where: L_d and L_q are q-axis and d-axis inductances; R is stator windings resistances; i_q,i_d are q-axis and d-axis currents; v_q and v_d are q-axis and d-axis voltages; ω_m is the rotor angular velocity; λ is the amplitude of the magnetic flux induced by the permanent magnets of the rotor in the stator phases; p is the number of pole pairs and T_e is eletromagnetic torque.

$$\frac{di_d}{dt} = \frac{1}{L_d}v_d - \frac{R}{L_d}i_d + \frac{L_q}{L_d}p\omega_m i_q \tag{14}$$

$$\frac{di_q}{dt} = \frac{1}{L_q}v_q - \frac{R}{L_q}i_q + \frac{L_d}{L_q}p\omega_m i_d - \frac{\lambda p \omega_m}{L_q} \tag{15}$$

$$T_e = 1.5p\left(\lambda i_q + (L_d - L_q) i_d i_q\right) \tag{16}$$

The motor's dynamic behavior is characterized based on the machine electrical parameters, which are given by the manufacturer and shown in Table 3.

Table 3. PMSM Model Parameters

Parameter	Value
Number of phases	3
Back EMF waveform	Sinusoidal
Rotor type	Salient-pole
Stator resistance R_s	0.0071 Ω
Inductances L_d, L_q	96.5 μH, 96.5 μH
Torque constant k_ϕ	0.43134 (Nm / A_{pk})
Rotor Inertia (J)	0.02521 kg.m^2
Viscous damping (F)	0.00281 N.m.s
Pole pairs p	10
Static friction T_f	0 N.m

FINITE CONTROL SET MODEL PREDICTIVE CONTROL

Initially developed in the 1970s by [21], the predictive control model consists of a set of discrete control techniques that employ optimization algorithms to select the control action based on prediction of the system's behavior. According to [22], the main elements of MPC control are: a) a mathematical model of the plant to be controlled, through a difference equation; b) the resolution of an optimal control problem, through the evaluation of a set of possible control actions, by defining a cost function that encompasses the actions and control objectives; c) a receding horizon policy, in which only the ideal control action, that is, the one presenting the smallest value of the cost function, is applied to the plant at each sampling instant. Due to the discrete nature of power converters, the optimization problem can be simplified, as there are a finite number of possible control actions to be implemented. Thus, the control action with the lowest cost is chosen and applied to the converter. Such is the basic functioning of the FCS-MPC (Finite Control Set MPC) technique or Model Predictive Control based on finite state sets. The FCS-MPC control strategy can handle multiple variables, disturbances, and control constraints, in addition to incorporating any characteristic that can be mathematically modeled in the cost function. This highlights the potential of this approach to overcome the challenges faced by traditional inverter control techniques.

The operating principle of the FCS-MPC technique can be understood through the example depicted in Fig. 6, where the control variable y_k, at the instant of sample time t_k, can be controlled through four different control actions (j_1, j_2, j_3 and j_4), to achieve the best match between y_{k+1} and the reference value y^* at time t_{k+1}. In the case illustrated in Fig. 6, for t_{k+1} the control action j_3 would be chosen, since it presents the lowest error between the predicted value of y_k and y^*, i.e., it has the lowest cost. This process repeats for the next samples so that the reference tracking is satisfactorily accomplished.

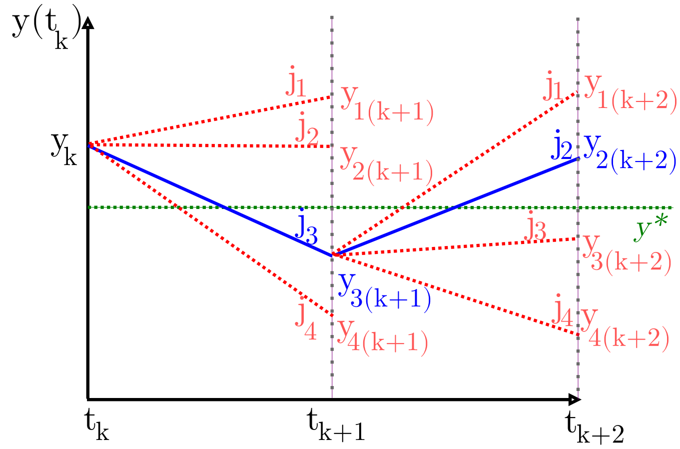

Figura 6. FCS-MPC control strategy example.

PROPOSED CONTROL STRATEGY

Figure 5 illustrates a control arrangement for an electric propulsion system that uses PMSM and FCS-MPC control. As can be seen, the reference speed of the PMSM shaft ω^* is defined from a driving cycle. The difference between ω^* and the instantaneous speed of the PMSM, defined by ω, is processed by a PI controller that defines the peak value I_s^* of the three-phase currents $i_a^*(t)$, $i_b^*(t)$, $i_c^*(t)$, which must be synthesized by the inverter and supplied to the PMSM, with the aim of matching ω^* and ω. These reference currents are obtained from reading the electrical angular displacement $\theta_e(t)$ of the PMSM. Thus, after a reference change using the Clarke transform (abc-$\alpha\beta$), for both the reference currents and the currents measured at the motor terminals, the FCS-MPC controller adjusts the driving condition of the transistors S_1-S_6 of the inverter bridge through the drive signals g_1-g_6. Subsequently, the inverter will convert the format of the

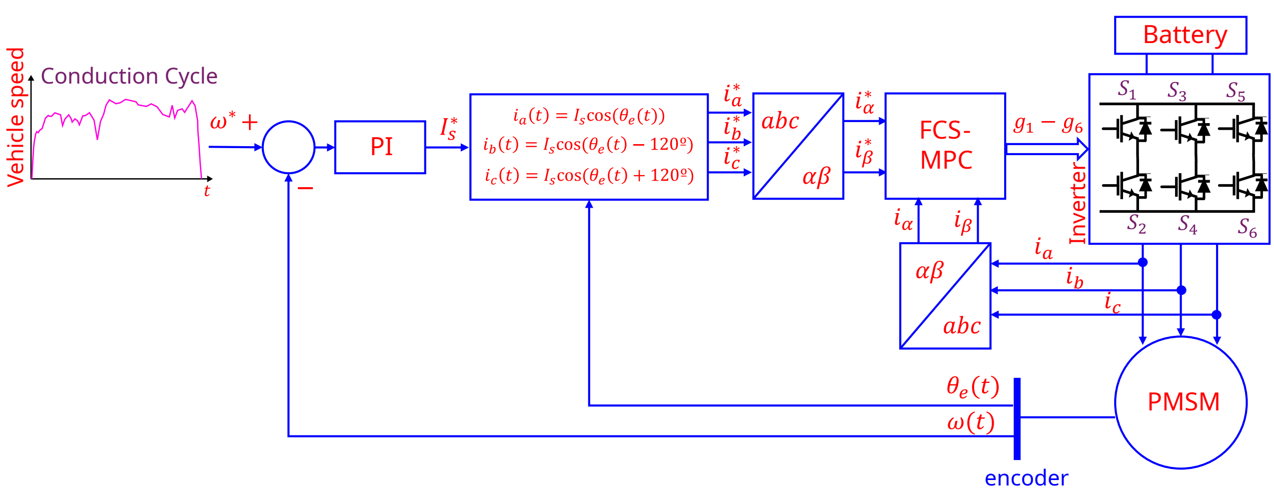

Figura 5. Proposed FCS-MPC control strategy for the PMSM drive.

electric energy available from the battery to the PMSM to meet the speed tracking control objectives.

RESULTS

Figure 7 presents the simulation results of the FCS-MPC controller applied to the PMSM drive system. Figure 7a shows the motor speed response under control compared to the reference profile. The solid blue line represents the reference speed, while the black dashed line indicates the response of the controlled system. It is observed that the controller accurately tracks the reference ramp, with nearly overlapping trajectories, demonstrating the effectiveness of the FCS-MPC in following the desired speed profile. Figure 7b presents the torque generated by the PMSM throughout the simulation. The torque adjusts effectively to accurately reproduce the desired speed trajectory, reaching a peak of 66.74 Nm. Additionally, a saturation behavior is observed near 1.1 s, where the torque decreases to maintain a constant speed, which is consistent with the system's stabilization phase.

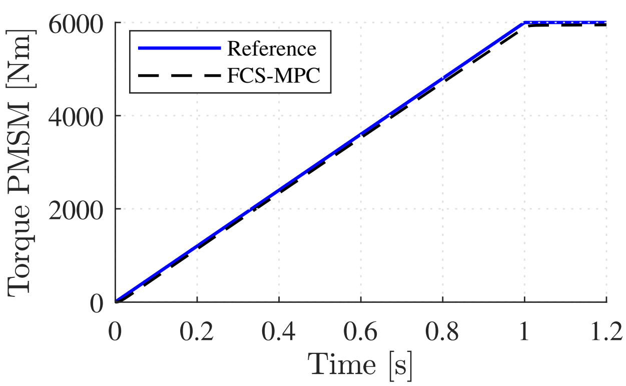

(a) PMSM Speed

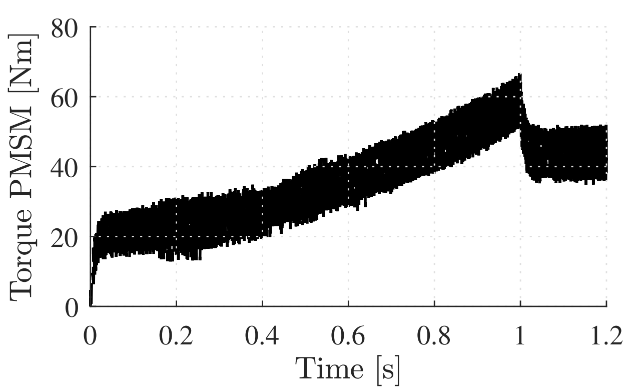

(b) PMSM Torque

Figura 7. Simulation of the FCS-MPC applied to the PMSM

Figure 8 shows the results of the FTP-75 driving cycle simulation, which is representative of typical urban traffic conditions. The solid blue line indicates the reference speed from the standard cycle, while the black dashed line represents the speed achieved by the vehicle controlled by the FCS-MPC strategy. It is observed that the trajectory of the controlled system consistently follows the reference throughout the entire cycle, demonstrating the controller's ability to accurately track the desired driving profile. The tracking performance is quantified by the root mean square (RMS) error, which was 0.0659 km/h, indicating a low deviation between the signals. Furthermore, the correlation coefficient between the curves reached 0.9998, highlighting the controller's effectiveness in replicating the reference cycle. These results confirm the FCS-MPC strategy as an effective approach for reproducing complex dynamic profiles typical of electric vehicle operation in urban environments.

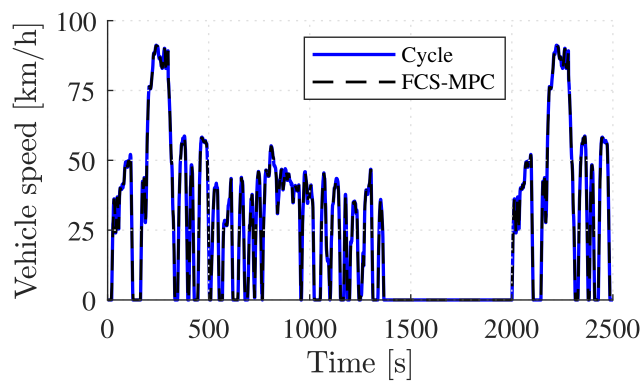

Figura 8. FCS-MPC simulation in FTP-75.

Figure 9 provides a detailed view of the speed signals presented in Fig. 8, focusing on the time interval between 162 s and 167 s. A slight deviation is observed between the reference speed and the vehicle's actual speed at the motor startup moment, reflecting the initial transition from inertia to motion. Despite this minor discrepancy, the response of the FCS-MPC controller quickly converges to the desired profile. This behavior highlights the control strategy's ability to handle rapid dynamic variations while maintaining performance even under transient conditions.

Figure 10 presents the results of the HWFET driving cycle simulation, commonly used to represent highway and non-urban traffic conditions. The solid blue line represents the reference speed from the standard cycle, while the black dashed line indicates the speed achieved by the vehicle controlled by the FCS-MPC strategy. It is observed that, although the HWFET cycle involves smoother accelerations and higher average speeds, the controlled system is able to accurately track the desired trajectory throughout the cycle. The RMS error was 0.0379 km/h, indicating solid control performance even under high-speed conditions. Additionally, the correlation coefficient between the speed profiles was 0.9999, further confirming the ability of the FCS-MPC to faithfully reproduce the reference cycle. These results demonstrate the robustness and versatility of the proposed control strategy, even under

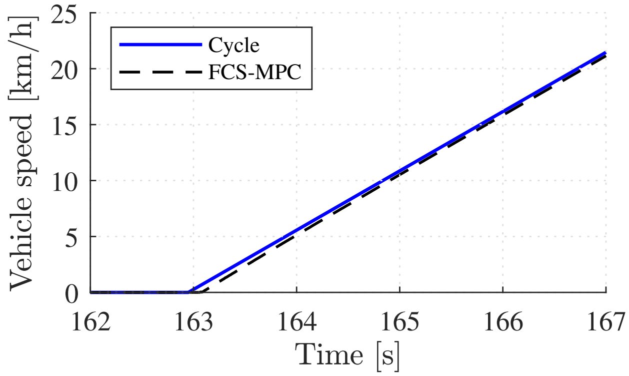

Figura 9. Speed response between 162 s and 167 s

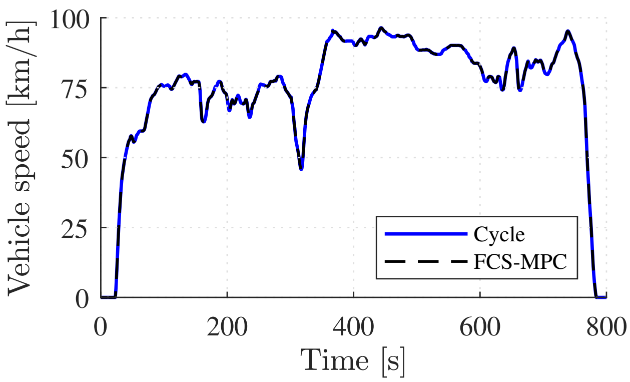

Figura 10. FCS-MPC simulation in HWFET

operational conditions distinct from those typical of urban environments.

CONCLUSION

Based on the work carried out, this study successfully achieved its proposed objectives by modeling and simulating a drive system based PMSM, taking into account vehicle dynamics. The implementation of the FCS-MPC strategy for motor current control proved to be effective, delivering a fast and robust dynamic response for the traction system. Validation through standard driving cycles allowed for performance evaluation of the proposed system, confirming its ability to accurately reproduce the desired speed profiles throughout operation. The FCS-MPC-controlled system achieved a root mean square (RMS) error of 0.0659 km/h for the FTP-75 cycle and 0.0379 km/h for the HWFET cycle, demonstrating its ability to accurately follow the desired speed profiles. These results highlight the potential of FCS-MPC as a promising control strategy for electric vehicle propulsion systems, contributing to the development of more efficient, reliable solutions aligned with the challenges of sustainable mobility.

ACKNOWLEDGMENT

This work was conducted with support from Paulista State University.

Referências

[1] L. Cai, W. Lv, L. Xiao, and Z. Xu, "Total carbon emissions minimization in connected and automated vehicle routing problem with speed variables," *Expert Systems with Applications*, vol. 165, p. 113910, 2021.
[2] L. Koch, M. Picerno, K. Badalian, S.-Y. Lee, and J. Andert, "Automated function development for emission control with deep reinforcement learning," *Engineering Applications of Artificial Intelligence*, vol. 117, p. 105477, 2023.
[3] F. Leach, G. Kalghatgi, R. Stone, and P. Miles, "The scope for improving the efficiency and environmental impact of internal combustion engines," *Transportation Engineering*, vol. 1, p. 100005, 2020.
[4] J. Liao, J. Hu, P. Chen, L. Zhu, Y. Wu, Z. Cai, H. Wu, and M. Wang, "Prediction of the transient emission characteristics from diesel engine using temporal convolutional networks," *Engineering Applications of Artificial Intelligence*, vol. 127, p. 107227, 2024.
[5] MOVER. (2025) Fundep fundac¸ao de apoio da ufmg. programa mobilidade verde e inovação - mover. [Online]. Available: https://www.programa-mover.com/programa-mover/
[6] H. Dong, J. Fu, Z. Zhao, Q. Liu, Y. Li, and J. Liu, "A comparative study on the energy flow of a conventional gasoline-powered vehicle and a new dual clutch parallel-series plug-in hybrid electric vehicle under nedc," *Energy Conversion and Management*, vol. 218, p. 113019, 2020.
[7] J. J. Eckert, T. P. Barbosa, F. L. Silva, V. R. Roso, L. C. Silva, and L. A. R. da Silva, "Optimum fuzzy logic controller applied to a hybrid hydraulic vehicle to minimize fuel consumption and emissions," *Expert Systems with Applications*, vol. 207, p. 117903, 2022.
[8] P. Kumar, H. K. Channi, and H. Singh, "A comprehensive review of electrical motors for electric mobility," in *2024 IEEE International Conference for Women in Innovation, Technology & Entrepreneurship (ICWITE)*. IEEE, 2024, pp. 130–135.
[9] S.-e. Kim and Y.-m. You, "Optimization of a permanent magnet synchronous motor for e-mobility using metamodels," *Applied Sciences*, vol. 12, no. 3, p. 1625, 2022.
[10] A. D. O. d. S. Dantas, A. F. O. d. A. Dantas, J. T. L. Campos, D. L. de Almeida Neto, and C. E. T. Dórea, "Pid control for electric vehicles subject to control and speed signal constraints," *Journal of Control Science and Engineering*, vol. 2018, no. 1, p. 6259049, 2018.
[11] M. A. Shamseldin, "Design of auto-tuning nonlinear pid tracking speed control for electric vehicle with uncertainty consideration," *World Electric Vehicle Journal*, vol. 14, no. 4, p. 78, 2023.
[12] M. H. Miranda, F. L. Silva, M. A. Lourenço, J. J. Eckert, and L. C. Silva, "Electric vehicle powertrain and fuzzy controller optimization using a planar dynamics simulation based on a real-world driving cycle," *Energy*, p. 121979, 2021.
[13] J. J. Eckert, L. C. Silva, F. G. Dedini, and F. C. Correa, "Electric vehicle powertrain and fuzzy control multi-objective optimization, considering dual hybrid energy storage systems," *IEEE Transactions on Vehicular Technology*, 2020.
[14] F. L. Silva, "Aprendizagem de máquinas aplicada à estratégia de gerenciamento de potência em veículos elétricos," Ph.D. dissertation, PHD Thesis, School of Mechanical Engineering- FEM, University of Campinas - UNICAMP, 2023.
[15] H. He, Y. Wang, R. Han, M. Han, Y. Bai, and Q. Liu, "An improved mpc-based energy management strategy for hybrid vehicles using v2v and v2i communications," *Energy*, vol. 225, p. 120273, 2021.
[16] M. H. Miranda, F. L. Silva, M. A. Lourenço, J. J. Eckert, and L. C. Silva, "Particle swarm optimization of elman neural network applied to battery state of charge and state of health estimation," *Energy*, vol. 285, p. 129503, 2023.
[17] G. Genta and L. Morello, *The automotive chassis: vol. 2: system design*. Springer, 2009.
[18] T. Gillespie, *Fundamentals of vehicle dynamics*. SAE international, 2021.
[19] R. N. Jazar, *Vehicle dynamics: theory and application*. Springer Science & Business Media, 2008.

[20] EMRAX d.o.o., "EMRAX 208 Electric Motor," https://emrax.com/e-motors/emrax-208/, 2025, accessed: 2025-05-15.
[21] J. Richalet, A. Rault, J. Testud, and J. Papon, "Model predictive heuristic control," *Automatica (journal of IFAC)*, vol. 14, no. 5, pp. 413–428, 1978.
[22] P. Karamanakos, E. Liegmann, T. Geyer, and R. Kennel, "Model predictive control of power electronic systems: Methods, results, and challenges," *IEEE Open Journal of Industry Applications*, vol. 1, pp. 95–114, 2020.